

# Different orbital occupation by an added single electron in 1,10-phenanthroline and its 3,4,7,8-tetramethyl derivative. Evidence from electron paramagnetic resonance spectroscopy of the anion radicals and of their dimesitylplatinum(II) complexes. X-Ray molecular structure of dimesityl(1,10-phenanthroline)platinum(II)

Axel Klein, Wolfgang Kaim,\* Eberhard Waldhör and Hans-Dieter Hausen

Institut für Anorganische Chemie der Universität, Pfaffenwaldring 55, D-70550 Stuttgart, Germany

In contrast to the anion radicals of 1,10-phenanthroline (phen) or its 4,7-dimethyl derivative (dmphen) with their  $^2B_1$  ground state, the 3,4,7,8-tetramethyl derivative tmphen $^{\cdot-}$  has a  $^2A_2$  ground state as evident from EPR/ENDOR measurements. The small  $\pi$  spin population at the potentially metal-coordinating nitrogen centres in the  $^2A_2$  species as opposed to the  $^2B_1$  state causes distinct spectroscopic effects in corresponding diorganoplatinum(II) complexes. The neutral compound (phen)PtMes $_2$ , Mes = mesityl, has been structurally characterized as a square planar Pt $^{II}$  complex with tightly protected axial sites: monoclinic, space group  $P2_1/c$ ,  $Z = 4$ ,  $a = 9.378(1)$ ,  $b = 15.791(2)$ ,  $c = 16.581(1)$  Å,  $\beta = 103.18(1)^\circ$ . All complexes (N $\wedge$ N)PtMes $_2$ , N $\wedge$ N = bpy (2,2'-bipyridine), phen, tmphen, dppz (dipyrido[3,2-*a*:2',3'-*c*]phenazine) and pdo (1,10-phenanthroline-5,6-dione) are oxidized to EPR-silent platinum(III) species and reduced to anion radical complexes. The latter clearly contain Pt $^{II}$  and heterocyclic anion radical ligands; however, they exhibit a trichotomous EPR behaviour. Whereas the radical complex [(phen)PtMes $_2$ ] $^{\cdot-}$  shows a rather low  $g_{iso}$ -value of 1.983 and distinct  $g$  anisotropy in frozen solution like the analogous complex of bpy $^{\cdot-}$ , the formally related [(tmphen)PtMes $_2$ ] $^{\cdot-}$  has an isotropic  $g$ -factor (2.0030) much closer to the free-electron value and a distinctly smaller  $g$  anisotropy. The phenanthroline-derived radical complexes [(pdo)PtMes $_2$ ] $^{\cdot-}$  and [(dppz)PtMes $_2$ ] $^{\cdot-}$  exhibit virtually no contribution from the coordinated heavy metal to the singly occupied MO ( $b_1$ ) which is mainly centred at the heteroatoms outside the phenanthroline  $\pi$  system.

## Introduction

Two very close lying molecular orbitals,  $a_2(\chi)$  and  $b_1(\psi)$  (Fig. 1), are available to accommodate the extra electron added to the widely used chelate ligand 1,10-phenanthroline (phen) and its derivatives.<sup>1-3</sup> High-resolution EPR measurements and their correlation with results from molecular orbital (MO) perturbation calculations of  $\pi$  spin populations have allowed an unambiguous determination of the spin distribution in phen $^{\cdot-}$  and dmphen $^{\cdot-}$  (dmphen = 4,7-dimethyl-1,10-phenanthroline),<sup>3</sup> both species were identified as  $^2B_1$  species.<sup>3</sup> The most obvious difference between the  $b_1(\psi)$  and  $a_2(\chi)$  orbitals is the much smaller orbital coefficient at the potentially coordinating nitrogen centres in the  $a_2$  MO (Fig. 1), which translates into a considerably smaller  $\pi$  spin population after electron addition.

The properties of the lowest unoccupied  $\pi$  MO (LUMO), in particular the  $\pi$  MO coefficients at the coordinating nitrogen atoms, are of considerable interest because these  $\pi(N)$  centres represent the 'gates' or the 'interface' for charge-transfer interactions between the unsaturated  $\pi$ -acceptor ligand and coordinated  $\pi$ -electron-rich metals.<sup>4,5</sup> For complexes between N-heterocycles and low-valent metals, the value of calculated Hückel MO coefficients  $c_N^2$ (LUMO) has been demonstrated for interpretations of NMR shifts,<sup>6</sup> metal-to-ligand charge transfer (MLCT) band intensities and solvatochromism,<sup>4,7</sup> reduction-potential shifts,<sup>4</sup> electron-transfer reactivity,<sup>5</sup> or comproportionation constants of mixed-valence dimers.<sup>8</sup>

In this work we report results obtained for the 3,4,7,8-tetramethyl derivative (tmphen $^{\cdot-}$ ) of 1,10-phenanthroline anion radical which demonstrate a switch to the  $^2A_2$  ground state, both for the free ligand radical and for the dimesitylplatinum(II) complex. The complexes [(N $\wedge$ N)PtMes $_2$ ] $^{\cdot-}$ , Mes = mesityl (2,4,6-trimethylphenyl), are unique in that they

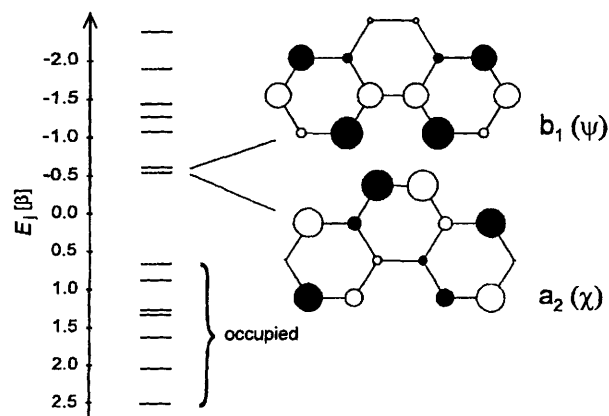


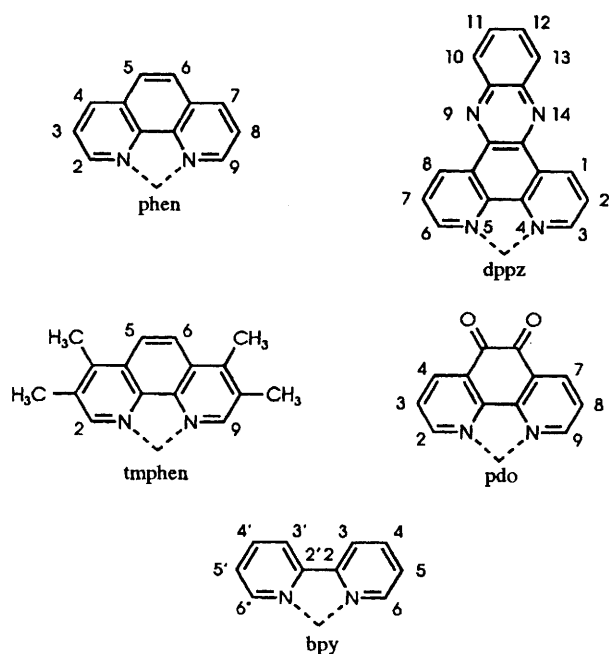
Fig. 1  $\pi$  Molecular orbital energies for 1,10-phenanthroline from a Hückel MO calculation ( $h_N = 0.5$ , all  $k = 1$ ) with the two low lying unoccupied MOs  $a_2(\chi)$  and  $b_1(\psi)$

contain an approximately square planar coordinated  $5d^{8+n}$  metal centre with both axial sites being effectively shielded.<sup>9,10</sup> As a consequence, (oxidative) addition reactivity is essentially prohibited and a persistent Pt $^{III}$  state can be generated.<sup>9,10</sup> The high spin-orbit coupling factor of platinum<sup>11</sup> can be expected to cause significant deviations of the  $g$ -factor and its components from the free-electron value of  $g_e = 2.0023$ , the extent of this deviation being particularly sensitive to the interaction between the heavy metal centre and the singly occupied MO of the ligand.<sup>12,13</sup> For comparison with either [(phen)PtMes $_2$ ] $^{\cdot-}$  or [(tmphen)PtMes $_2$ ] $^{\cdot-}$  we include results obtained for [(N $\wedge$ N)-PtMes $_2$ ] $^{\cdot-}$ , N $\wedge$ N = dipyrido[3,2-*a*:2',3'-*c*]phenazine (dppz),

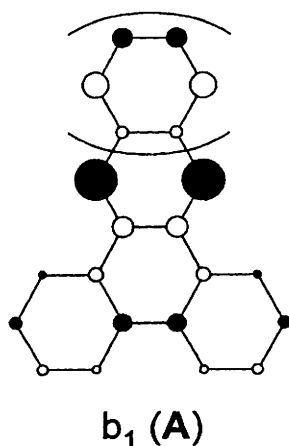
**Table 1** EPR coupling constants<sup>a</sup> of 1,10-phenanthroline anion radicals

Anion radical	$a(^{14}\text{N})$	$a(^1\text{H})^d$
phen <sup>•-</sup> <sup>b</sup>	0.280	0.041(H <sup>2</sup> ), 0.360(H <sup>3</sup> ), 0.280(H <sup>4</sup> ), 0.041(H <sup>5</sup> )
dmphen <sup>•-</sup> <sup>b</sup>	0.262	0.054(H <sup>2</sup> ), 0.428(H <sup>3</sup> ), 0.112(H <sup>4</sup> ), 0.054(H <sup>5</sup> )
tmphen <sup>•-</sup> <sup>c</sup>	0.073	0.417(H <sup>2</sup> ), <sup>f</sup> <0.005(H <sup>3</sup> ), <sup>e,f</sup> 0.336(H <sup>4</sup> ), <sup>e,f</sup> 0.449(H <sup>5</sup> ) <sup>f</sup>

<sup>a</sup> Coupling constants in mT. <sup>b</sup> From reduction with K in tetrahydrofuran (THF) at 300 K (ref. 3). <sup>c</sup> From reduction with K in THF/[2.2.2]cryptand at 240 K. <sup>d</sup> Assignments following Hückel molecular orbital (HMO)  $\pi$  spin populations (see text and Fig. 1). <sup>e</sup> Methyl proton hyperfine splitting. <sup>f</sup> Confirmed by ENDOR spectroscopy at 240 K.



1,10-phenanthroline-5,6-dione (pdo) or bpy. Whereas the latter is clearly a  $^2\text{B}_1$  species<sup>9,10</sup> because of the destabilized  $a_2(\chi)$  MO in 2,2'-bipyridine,<sup>14</sup> the two former complexes can be expected to have the unpaired electron localized in the phenazine<sup>15,16</sup> or  $\alpha$ -semidione<sup>17</sup> parts of the radical ligand, respectively. The orbital involved there is of  $b_1$  symmetry (A) but lacks any significant MO coefficients at the coordinating nitrogen centres.<sup>15-17</sup>



## Results and discussion

### Tmphen radical anion

Tmphen is reduced to a green paramagnetic solution by elemental potassium in tetrahydrofuran (THF) which contains

small amounts of [2.2.2]-cryptand in order to avoid coordination of the resulting  $\text{K}^+$ . At 240 K, this solution exhibits well resolved EPR (Fig. 2) and electron-nuclear double resonance (ENDOR) spectra. The presence of *three* large  $^1\text{H}$  coupling constants (ENDOR) and of only one small  $^{14}\text{N}$  hyperfine splitting (EPR) already suggests an occupation of the  $a_2$  MO by the single electron, a  $^2\text{B}_1$  species like phen<sup>•-</sup> or dmphen<sup>•-</sup> (Table 1)<sup>3</sup> would require large  $a(^{14}\text{N})$  values and only two splitting constants  $a(^1\text{H}) > 0.1$  mT. The EPR spectrum of tmphen<sup>•-</sup> is thus reproducible (Fig. 2) assuming the coupling constants from Table 1 which agree very well with the Hückel MO coefficients as depicted in Fig. 1. In particular, there is virtually no spin population at the 3,8-positions and the highest  $\pi$  spin population resides at the non-methylated CH centres in the 2,9- and 5,6-positions. The small spin population at the nitrogen centres is also evident from the rather low isotropic  $g$ -value of 2.0027 for tmphen<sup>•-</sup>; non-methylated phen<sup>•-</sup> has  $g = 2.0030$  because of stronger contributions from the nitrogen atoms with their higher spin-orbit coupling constant relative to carbon atoms.<sup>11</sup>

It is remarkable that the mere substitution of hydrogen by methyl substituents in the 3,8-positions is sufficient to cause an orbital crossing<sup>3</sup>  $b_1/a_2$  on going from dmphen to tmphen (Table 1). However, it should be noted that the  $b_1$  MO has large  $\pi$  MO coefficients at the 3,8-positions (Fig. 1) so that the introduction of electron-donating methyl groups destabilizes this orbital. The  $a_2$  MO, on the other hand, has rather small  $\pi$  MO coefficients at those positions, leaving the energy of this MO largely unchanged upon substitution. Correspondingly parametrized Hückel MO calculations can reproduce such behaviour, whereas AM1 calculations in standard parametrization failed to confirm the experimental results for geometry-optimized phenanthroline systems. Exploratory studies indicate that successful *ab initio* approaches to this problem require a rather extensive basis set and the inclusion of polarization functions.

### Properties of neutral complexes $(\text{N}^{\wedge}\text{N})\text{PtMes}_2$

The complexes with  $\text{N}^{\wedge}\text{N} = \text{bpy}$ , phen, tmphen, dppz and pdo were obtained from the heterocyclic ligand and  $(\text{DMSO})_2\text{-PtMes}_2$  (DMSO = dimethyl sulfoxide) as described previously.<sup>9,10</sup> To study the influence of the more rigid phenanthroline ligand as compared with 2,2'-bipyridine, we determined the molecular structure of (phen)PtMes<sub>2</sub> in the crystal. Using SHELXTL PC package<sup>18</sup> the structure was solved by direct methods followed by a combination of Fourier synthesis and least-squares refinements. Bond distances and angles are given in Table 2. The molecular structure is depicted in Fig. 3 with the atomic labelling.

Structural comparison between (bpy)PtMes<sub>2</sub><sup>9</sup> and (phen)PtMes<sub>2</sub> reveals few essential differences. The virtually planar coordination at the metal and the effective axial shielding by the *ortho* methyl groups of the mesityl ligands are very similar; however, the NPtN angle is a bit larger for the phenanthroline system because of the enforced planarity of the heterocycle. In contrast, (bpy)PtMes<sub>2</sub> has a slightly twisted bpy ligand with a dihedral angle of 5.7° between the pyridyl planes and a smaller

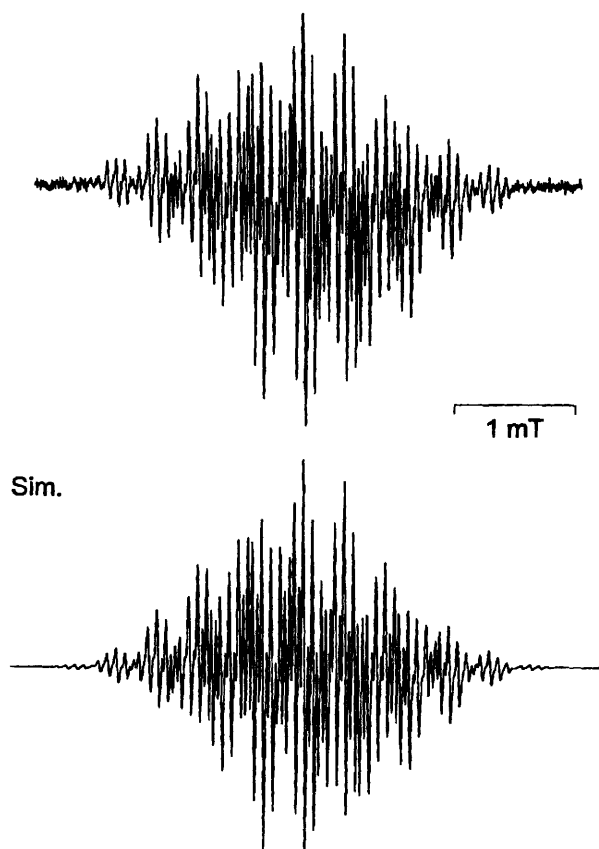


Fig. 2 EPR spectrum of  $\text{tmphen}^{\bullet-}$  as generated by reduction with potassium at 240 K in THF/[2.2.2]cryptand solution, accompanied by a computer simulation with the data from Table 1

Table 2 Selected bond lengths (pm) and angles ( $^{\circ}$ ) for  $(\text{phen})\text{PtMes}_2$

Pt–C(1)	201.7(5)	C(1)–Pt–C(10)	94.4(2)
Pt–C(10)	201.5(5)	C(1)–Pt–N(1)	94.0(2)
Pt–N(1)	210.3(4)	C(10)–Pt–N(1)	170.9(2)
Pt–N(2)	210.8(4)	C(1)–Pt–N(2)	173.1(2)
N(1)–C(19)	133.8(7)	C(10)–Pt–N(2)	92.5(2)
N(1)–C(30)	137.2(7)	N(1)–Pt–N(2)	79.2(2)
C(19)–C(20)	138.6(8)	Pt–C(1)–C(2)	123.4(4)
C(20)–C(21)	136.2(9)	Pt–C(1)–C(6)	120.8(4)
C(21)–C(22)	141.3(8)	Pt–C(10)–C(11)	120.9(4)
C(22)–C(23)	143.1(9)	Pt–C(10)–C(15)	123.2(4)
C(22)–C(30)	140.4(7)	Pt–N(1)–C(19)	129.2(4)
C(23)–C(24)	134.6(8)	Pt–N(1)–C(30)	113.2(3)
C(24)–C(25)	142.5(7)	C(19)–N(1)–C(30)	117.5(4)
C(25)–C(26)	140.1(8)	Pt–N(2)–C(28)	129.2(4)
C(25)–C(29)	142.0(7)	Pt–N(2)–C(29)	112.8(3)
C(26)–C(27)	138.0(8)	C(28)–N(2)–C(29)	118.1(5)
C(27)–C(28)	139.4(8)		
C(28)–N(2)	132.7(7)		
N(2)–C(29)	136.2(6)		
C(29)–C(30)	142.8(7)		
Average bond lengths (pm)			
C–C (Mes ring)	140.1	[137.8(9)–143.0(8)]	
C–C (Mes Me)	151.5	[150.2(9)–152.7(10)]	
Average bond angles ( $^{\circ}$ )			
C–C–C (Mes)	120.0	[115.2(4)–123.3(6)]	
C–C–C (phen)	120.05	[117.2(5)–124.3(5)]	
N–C–C (phen)	121.01	[116.7(4)–123.4(5)]	

NPtN bond angle of  $77.8^{\circ}$ .<sup>9</sup> The Pt–N and Pt–C bond lengths are not significantly different between both molecules, the 1,10-phenanthroline ligand exhibits a typical bond-length altern-

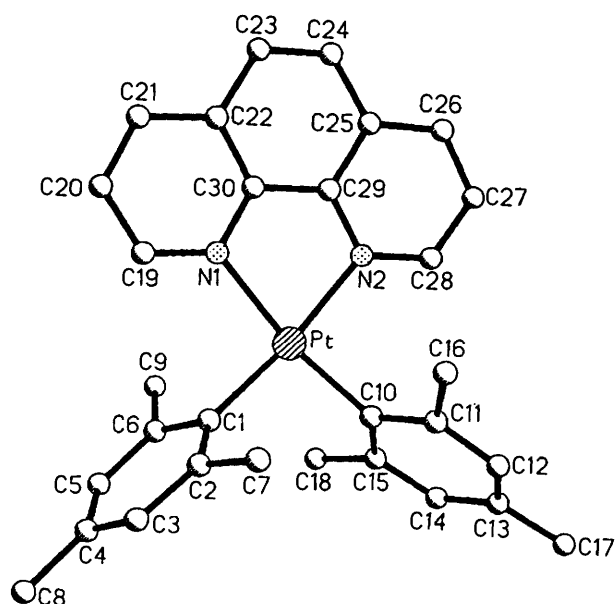


Fig. 3 Molecular structure of  $(\text{phen})\text{PtMes}_2$  in the crystal

ation in the homocyclic ring with a close-to-'olefinic' bond between C(23) and C(24).

The similarity between  $(\text{bpy})\text{PtMes}_2$ <sup>9</sup> and  $(\text{phen})\text{PtMes}_2$  pertains also to their optical absorption and emission and to their electrochemical behaviour.<sup>10</sup> Whereas the  $\text{Pt}^{\text{III}}$  complexes of  $\alpha$ -diimine ligands are well known to exhibit MLCT absorption and emission,<sup>10,19,20</sup> the occurrence of reversible one-electron reduction *and* oxidation processes is unusual.<sup>20</sup> The origin for this cyclic voltammetrically detectable behaviour lies in the axial protection (Fig. 2) of the oxidized, *i.e.*  $\text{Pt}^{\text{III}}$ , metal centre by the mesityl groups against the addition of nucleophiles such as the solvent.<sup>9,10,20</sup> One-electron reduction, on the other hand, produces  $\text{Pt}^{\text{II}}$  complexes of the heterocyclic anion radical ligands  $(\text{N}^{\wedge}\text{N})^{\bullet-}$ , a well known type of radical species.<sup>9,10,20–22</sup> In agreement with this notion, there is usually<sup>9,10</sup> a reversible second one-electron reduction involving the ligand dianion (Table 3).

Whereas the oxidation potentials show the expected<sup>10</sup> little variation, the reduction potentials of the complexes  $(\text{N}^{\wedge}\text{N})\text{PtMes}_2$  have to be viewed in comparison with those of the free ligands (Table 3). When compared with the compounds with  $\text{N}^{\wedge}\text{N} = \text{bpy}$  and phen, the complexes with  $\text{N}^{\wedge}\text{N} = \text{dppz}$  and pdo show only small effects of the  $\text{PtMes}_2$  coordination;  $(\text{tmphen})\text{PtMes}_2$  exhibits an intermediate position. Shifts of ligand-based redox potentials on coordination of electrophilic metal centres correlate with the MO coefficients at the coordinating  $\pi$  centres within a series of structurally related ligands.<sup>4</sup> The observed results suggest that the complexes  $[(\text{N}^{\wedge}\text{N})\text{PtMes}_2]^{\bullet-}$  with  $\text{N}^{\wedge}\text{N} = \text{bpy}$  and phen have the unpaired electron in an MO with sizeable  $\pi$  MO coefficients at the metal-binding nitrogen centres, most probably the  $b_1(\psi)$  orbital (Fig. 1), like the corresponding free ligand radical anions.<sup>3</sup> The smaller effect for the  $\text{tmphen}$  species supports the notion that the complex of  $\text{tmphen}$  anion radical is a  $^2A_2$  species with small MO coefficients at the  $\pi$  centres 1 and 10. Finally, the anionic complexes with  $\text{dppz}$  and pdo ligands probably have the single electron in the heteroatom-centred  $b_1$  MO (A) with its vanishing  $\pi$  spin population at the coordinating nitrogen centres. EPR studies of ion pairs and complexes of  $\text{pdo}^{\bullet-}$ <sup>17</sup> and  $\text{dppz}^{\bullet-}$ <sup>16,23</sup> have indeed revealed that the unpaired electron resides predominantly in the semidione ( $\text{pdo}^{\bullet-}$ ) or phenazine moieties ( $\text{dppz}^{\bullet-}$ ), respectively. Although all three ligand

**Table 3** Redox potentials<sup>a</sup> of ligands N<sup>^</sup>N and complexes (N<sup>^</sup>N)PtMes<sub>2</sub>

N <sup>^</sup> N	Ligand		Complex		
	<i>E</i> <sub>red</sub>	<i>E</i> <sub>ox</sub>	<i>E</i> <sub>red1</sub>	<i>E</i> <sub>red2</sub>	Solvent <sup>b</sup>
phen	-2.55 (67)	0.45 (75)	-1.93 (61)	-2.60 (120)	MeCN
bpy	-2.60 (63)	0.45 (60)	-2.05 (60)	-2.73 (80)	THF
tmphen	-2.68 (120)	0.42 (79)	-2.28 (74)	-2.91 (111)	THF
dppz	-1.75 (78)	0.49 (67)	-1.50 (62)	-2.24 (95)	THF
pdo	-0.87 (82)	0.53 (66)	-0.64 (60)	-0.86 (56)	MeCN

<sup>a</sup> From cyclic voltammetry at 100 mV s<sup>-1</sup> scan rate. Potentials in V vs. Fc<sup>+/0</sup>, peak potential differences in mV (in parentheses). <sup>b</sup> Solutions 0.1 mol dm<sup>-3</sup> in Bu<sub>4</sub>NPF<sub>6</sub>.

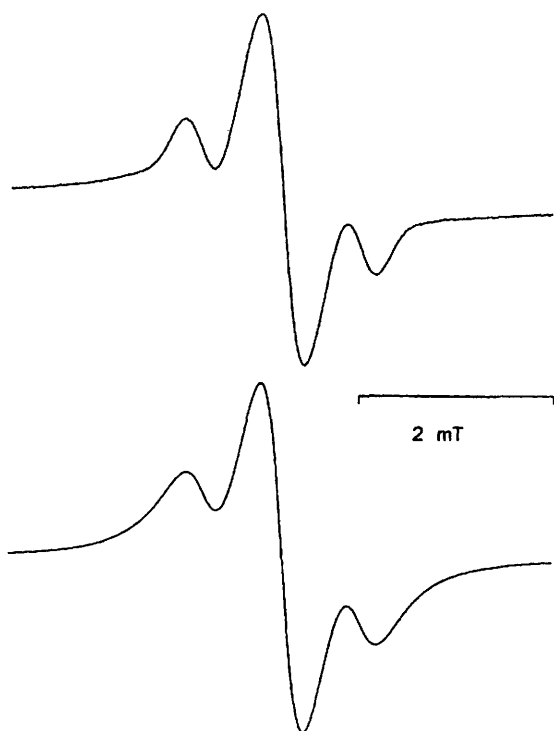


**Fig. 4** EPR spectrum of [(tmphen)PtMes<sub>2</sub>]<sup>•-</sup> as generated electrochemically in THF/0.1 mol dm<sup>-3</sup> Bu<sub>4</sub>NPF<sub>6</sub> at 293 K, accompanied by a computer simulation: *a*(Pt) = 1.6 mT, linewidth 0.5 mT

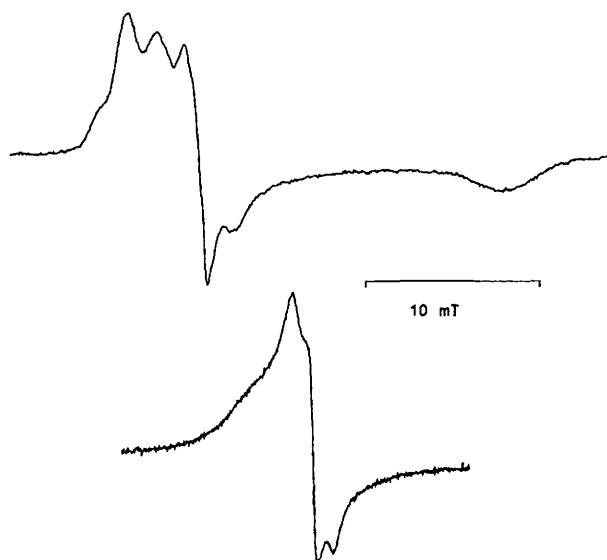


**Fig. 5** EPR spectra of [(phen)PtMes<sub>2</sub>]<sup>•-</sup> (top) and [(tmphen)PtMes<sub>2</sub>]<sup>•-</sup> (bottom) at 110 K in frozen THF/0.1 mol dm<sup>-3</sup> Bu<sub>4</sub>NPF<sub>6</sub>

radical anions, tmphen<sup>•-</sup>, dppz<sup>•-</sup> and pdo<sup>•-</sup>, do not have the b<sub>1</sub>(ψ) as singly occupied MO (SOMO), the coordination of metal or other electrophiles could change the orbital sequence by stabilizing this particular MO.<sup>24</sup>

#### EPR spectroscopy of radical complexes [(N<sup>^</sup>N)PtMes<sub>2</sub>]<sup>•-</sup>

In contrast to the Pt<sup>III</sup>-containing complex cations which remain EPR-silent down to 3 K because of very rapid relaxation processes,<sup>10</sup> the monoanionic complexes exhibit EPR spectra in fluid and glassy frozen solution (Figs. 4 and 5).

In fluid solution at ambient temperatures, the complex anions with N<sup>^</sup>N = dppz and pdo exhibit resolved N<sup>^</sup>N ligand hyperfine structure, no detectable <sup>195</sup>Pt hyperfine coupling, and an isotropic *g*-factor close to the free-ligand value; *g*<sub>iso</sub> of pdo<sup>•-</sup> is 2.0049. Ligand hyperfine structure is not resolved for [(tmphen)PtMes<sub>2</sub>]<sup>•-</sup>; however, the *g*<sub>iso</sub>-value of 2.0030 and the relatively<sup>10,21</sup> small <sup>195</sup>Pt hyperfine coupling (Fig. 4) still suggest occupation of the a<sub>2</sub> orbital by the unpaired electron. In contrast, the complex anions with N<sup>^</sup>N = phen or bpy exhibit EPR spectra with rather broad lines centred at *g*<sub>iso</sub> < 2 (Table 4); a large isotropic <sup>195</sup>Pt splitting of 4.0 mT could be detected for the bpy complex.<sup>10</sup>

The unresolved broad EPR signal of [(phen)PtMes<sub>2</sub>]<sup>•-</sup> can be understood by considering the rather large *g* anisotropy of this species in frozen solution (Fig. 5). Although this is clearly not a platinum(I) complex with a 5d<sup>9</sup> configuration (which should have *g*<sub>1</sub> ≫ *g*<sub>2,3</sub> > *g*<sub>electron</sub>),<sup>21,22</sup> there is a particularly low *g*<sub>3</sub>-value which suggests some appreciable contribution of the heavy metal centre with its large spin-orbit coupling constant to the singly occupied MO. The *g* anisotropy in frozen solution is slightly smaller for the bpy complex, with a similar pattern *g*<sub>1</sub> > *g*<sub>2</sub> ≈ *g*<sub>electron</sub> ≫ *g*<sub>3</sub>. Both bpy and phen containing anions thus reveal an involvement of the b<sub>1</sub> MO with its high MO coefficients at the coordinating N centres (Fig. 1) *via* the observed strong metal/ligand interaction.

Owing to the radical character of the paramagnetic complexes presented here, the <sup>195</sup>Pt hyperfine components *a*<sub>1</sub>-*a*<sub>3</sub> could be determined only in a few instances where magnitude, linewidth and lack of overlap of *g* components allowed such a measurement. EPR studies at higher frequencies will be necessary to obtain relevant information.

The pdo and dppz containing radical complexes exhibit very small *g* anisotropy as is typical for purely organic radicals and radical ions.<sup>13,25</sup> For [(tmphen)PtMes<sub>2</sub>]<sup>•-</sup>, this anisotropy is detectable but smaller by about a magnitude when compared with that of the non-methylated analogue (Fig. 5, Table 4). We therefore conclude that this complex is a <sup>2</sup>A<sub>2</sub> species which has a slightly higher contribution from the metal to the SOMO than the pdo and dppz analogues. While the latter contain ligands with low-lying heteroatom-centred b<sub>1</sub> MOs (A),<sup>16,17</sup> the tmphen radical complex has to use the a<sub>2</sub> orbital to accommodate the extra electron.

**Table 4** EPR data<sup>a</sup> of anion radical complexes<sup>b</sup> [(N<sup>^</sup>N)PtMes<sub>2</sub>]<sup>-</sup>

N <sup>^</sup> N	<i>g</i> <sub>iso</sub>	<i>g</i> -Components <sup>c</sup>			$\Delta g^d$	<i>a</i> (Pt) <sub>iso</sub>	<i>a</i> (Pt)-Components <sup>c</sup>			Further hyperfine splitting
		<i>g</i> <sub>1</sub>	<i>g</i> <sub>2</sub>	<i>g</i> <sub>3</sub>			<i>a</i> <sub>1</sub>	<i>a</i> <sub>2</sub>	<i>a</i> <sub>3</sub>	
phen <sup>e</sup>	1.983	2.0304	2.0048	1.9070	1234	< 4.5	2.0	3.1	< 2.5	
bpy <sup>f</sup>	1.9898	2.0312	2.0071	1.9340	972	4.0	5.2	3.8	< 3.4	
tmphen <sup>e</sup>	2.0030	2.0101	2.0031	1.9963	141	1.6		n.d.		
dppz <sup>f</sup>	2.0035	2.0069	2.0039	2.0039 <sup>g</sup>	30	< 0.2		n.d.		0.52 <sup>g</sup>
pdo <sup>e</sup>	2.0045	2.0045	2.0045	2.0045	< 20	< 0.4		n.d.		<i>h</i>

<sup>a</sup> Coupling constants for nuclei <sup>1</sup>H, <sup>14</sup>N or <sup>195</sup>Pt (*I* = 1/2, 33.8% nat. abundance) in mT. Data from graphical spectra analysis, errors estimated for *a*<sub>1</sub>, *a*<sub>2</sub>, *a*<sub>3</sub> at  $\pm 0.3$  mT, for *g*<sub>1</sub>, *g*<sub>2</sub>, *g*<sub>3</sub> at  $\pm 0.0007$ . <sup>b</sup> Generated from neutral precursors by cathodic reduction in 1,2-dichloroethane/0.1 mol dm<sup>-3</sup> Bu<sub>4</sub>NPF<sub>6</sub> (bpy and dppz complexes) or THF/0.1 mol dm<sup>-3</sup> Bu<sub>4</sub>NPF<sub>6</sub>. <sup>c</sup> At 110 K in glassy frozen solution. <sup>d</sup>  $\Delta g = (g_1 - g_3) \times 10^4$ . <sup>e</sup> This work. <sup>f</sup> From ref. 10, glassy frozen solution spectra measured at 150 K. <sup>g</sup> Quintet coupling *a*(N<sup>9,14</sup>) at 293 K. <sup>h</sup> Hyperfine structure at 293 K: *a*(<sup>14</sup>N) = 0.0635, *a*(H<sup>3</sup>) = 0.120, *a*(H<sup>2,4</sup>) = 0.081 mT. n.d. = not determined.

### Conclusions

This study reveals for the first time that 1,10-phenanthroline anion radicals *can* have the *a*<sub>2</sub> orbital as SOMO instead of *b*<sub>1</sub>. Starting from the <sup>2</sup>B<sub>1</sub> ions phen<sup>-</sup> and 4,7-dimethylated dmphen<sup>-</sup>, the additional 3,8-dimethyl substitution in tmphen<sup>-</sup> causes the switch to a <sup>2</sup>A<sub>2</sub> species. Having taken advantage of the high spin-orbit coupling constant of radical-bound platinum(II) we conclude similarly that the complex [(N<sup>^</sup>N)PtMes<sub>2</sub>]<sup>-</sup> of unmethylated 1,10-phenanthroline radical anion has the *b*<sub>1</sub> orbital singly occupied with its high MO coefficient at the metal-binding nitrogen centres, whereas the *a*<sub>2</sub> MO is singly occupied in the radical complex of tmphen. The radical complexes of the dppz and pdo ligands are <sup>2</sup>B<sub>1</sub> species which have the spin predominantly centred at the heteroatoms (O or N) outside the phenanthroline system.

### Experimental

EPR and ENDOR spectra were recorded in the X band on a Bruker System ESP 300 equipped with an ENI A500 RF amplifier, a Bruker ER033 field-frequency lock, a Bruker ER033M gaussmeter and an HP 5350B microwave counter. <sup>1</sup>H NMR spectra were taken on a Bruker AC 250 spectrometer. UV-Visible and near IR absorption spectra were recorded on Shimadzu UV160 and Bruins Instruments Omega 10 spectrophotometers. A Perkin-Elmer fluorescence spectrometer LS-3B served to record emission spectra. Cyclic voltammetry was carried out in acetonitrile/- or tetrahydrofuran/0.1 mol dm<sup>-3</sup> Bu<sub>4</sub>NPF<sub>6</sub> using a three-electrode configuration (glassy carbon electrode, Pt counter electrode, Ag/AgCl reference) and a PAR 273 potentiostat and function generator. The ferrocene/ferrocenium couple served as internal reference. Sealed glass tubes (tmphen<sup>-</sup>) or two-electrode electrolytic cells were used for generation of radical anions.

Synthetic procedures for the ligands dppz<sup>15,16</sup> and pdo<sup>17</sup> and for the complexes (N<sup>^</sup>N)PtMes<sub>2</sub> have been described.<sup>9,10</sup> The other ligands and reagents were used as commercially available. Solvents and electrolytes were rigorously dried before use.

#### (phen)PtMes<sub>2</sub>

Yellow-orange crystals (Found: C, 58.9; H, 4.9; N, 4.5. C<sub>30</sub>H<sub>30</sub>N<sub>2</sub>Pt requires C, 58.72; H, 4.93; N, 4.56%); absorption  $\lambda_{\max}$ (toluene)/nm 500, 447, 420 and 296; emission  $\lambda_{\max}$ (toluene)/nm 622 (excitation at 488 nm);  $\delta_{\text{H}}$ (250 MHz; [<sup>2</sup>H<sub>6</sub>]DMSO) 2.14 (6 H, s, *p*-Me), 2.38 (12 H, t, *J*<sub>HPt</sub> 6.0, *o*-Me), 6.56 (4 H, t, *J*<sub>HPt</sub> 14.9, CH<sub>Mes</sub>), 7.98 (2 H, dd, *J* 5.20 and 8.26, 3- and 8-H), 8.24 (2 H, s, 5- and 6-CH), 8.46 (2 H, dd, *J* 1.35 and 5.20, 4- and 7-H) and 8.96 (2 H, dd, *J* 1.35 and 8.26, 2- and 9-H).

#### (tmphen)PtMes<sub>2</sub>

Yellow crystals (Found: C, 60.0; H, 5.6; N, 4.1. C<sub>34</sub>H<sub>38</sub>N<sub>2</sub>Pt requires C, 60.97; H, 5.72; N, 4.18%); absorption  $\lambda_{\max}$ (toluene)/

nm 523sh, 468, 443, 398, 345, 326sh and 303; emission  $\lambda_{\max}$ (toluene)/nm 586 (excitation at 500 nm);  $\delta_{\text{H}}$ (250 MHz; [<sup>2</sup>H<sub>6</sub>]DMSO) 2.29 (6 H, s, 3- and 8-Me), 2.35 (6 H, s, *p*-Me), 2.37 (12 H, s, *o*-Me), 2.64 (6 H, s, 4- and 7-Me), 6.55 (4 H, s, CH<sub>Mes</sub>), 8.18 (2 H, s, 5- and 6-H) and 8.35 (2 H, s, 2- and 9-H).  $\delta$ (250 MHz; CD<sub>2</sub>Cl<sub>2</sub>) 2.22 (6 H, t, *J*<sub>HPt</sub> 4.2, 3- and 8-Me), 2.41 (6 H, s, *p*-Me), 2.45 (12 H, t, *J*<sub>HPt</sub> 5.2, *o*-Me), 2.61 (6 H, s, 4- and 7-Me), 6.66 (4 H, t, *J*<sub>HPt</sub> 14.6, CH<sub>Mes</sub>), 8.12 (2 H, s, 5- and 6-CH) and 8.36 (2 H, t, *J*<sub>HPt</sub> 21.8, 2- and 9-H).

#### (pdo)PtMes<sub>2</sub>

Dark crystals (Found: C, 55.65; H, 4.6; N, 4.2. C<sub>28</sub>H<sub>28</sub>N<sub>2</sub>O<sub>2</sub>Pt requires C, 55.98; H, 4.38; N, 4.35%); absorption  $\lambda_{\max}$ (toluene)/nm 562sh, 503, 439sh, 413, 377, 358, 341 and 307; emission  $\lambda_{\max}$ (toluene)/nm 585 (excitation at 500 nm);  $\delta_{\text{H}}$ (250 MHz; [<sup>2</sup>H<sub>6</sub>]DMSO) 2.16 (6 H, s, *p*-Me), 2.36 (12 H, s, *o*-Me), 6.54 (4 H, t, *J*<sub>HPt</sub> 15.6, CH<sub>Mes</sub>), 7.84 (2 H, dd, *J* 5.58 and 7.75, 3- and 8-H), 8.29 (2 H, d, *J* 5.58, 4- and 7-H), 8.74 (2 H, d, *J* 7.75, 2- and 9-H).

#### Crystal structure determination of (phen)PtMes<sub>2</sub>

Suitable crystals were obtained by slow evaporation of the solvent from a 1,2-dichloroethane solution. Single-crystal X-ray diffraction measurements were performed at 173 K on a Siemens P4 automatic four-circle diffractometer using graphite-monochromatized Mo-K $\alpha$  radiation. The cell parameters were obtained by least-squares fit of 38 accurately centred reflections with  $2\theta = 21$ – $25^\circ$ , found by a random search of the reciprocal lattice. 6646 Reflections were collected with variable speed (3–60°/min),  $\omega/2\theta$  mode with  $1.4^\circ$   $\omega$  scan width ( $3^\circ \leq 2\theta \leq 58^\circ$ ;  $h = 0$ – $12$ ,  $k = 0$ – $21$ ,  $l = -22$  to 22) of which 6286 reflections were independent and 4917 observed [ $F > 4\sigma(F)$ ]. The intensities of two standard reflections, monitored after every 98 measurements, remained unchanged with only statistical fluctuations. Lorentz and polarization effects were corrected and a semiempirical absorption correction was applied (min/max transmission factors 0.37/0.91).

**Crystal data.** C<sub>30</sub>H<sub>30</sub>N<sub>2</sub>Pt, *M* = 613.7, monoclinic, space group *P*2<sub>1</sub>/*c* (ITC No. 14), *a* = 937.8(1), *b* = 1579.1(2), *c* = 1658.1(1) pm;  $\beta = 103.18(1)^\circ$ , *V* = 2390.8(4)  $\times 10^6$  pm<sup>3</sup>, *Z* = 4, *D*<sub>c</sub> = 1.705 g cm<sup>-3</sup>, *F*(000) = 1208,  $\mu$ (Mo-K $\alpha$ ) = 58.9 cm<sup>-1</sup>.

**Structure analysis and refinement.** The structure was solved by 'direct methods' and subsequently completed by a combination of least-squares techniques and Fourier syntheses. All non-hydrogen atoms were refined anisotropically. The hydrogen atoms were located in calculated positions with C–H bond lengths of 96 pm and fixed isotropic thermal parameters (800 pm<sup>2</sup>). The structure model was refined by full-matrix least-squares (298 parameters) minimizing the function  $\sum w(F_o - F_c)^2$ , converging to  $R_1 = \sum(|F_o| - |F_c|)/\sum|F_o| = 0.038$  and  $R_2 = [\sum w(|F_o| - |F_c|)^2/\sum w F_o^2]^{1/2} = 0.037$  with the final

weighting scheme  $w = 1/[\sigma^2(F_o) + 0.0003F_o^2]$  and goodness of fit =  $[w(|F_o| - |F_c|)^2/n - p]^{1/2} = 1.33$ ; electron-density residuals for the last difference map are 3.31 and  $-2.26 \text{ e} \times 10^{-6} \text{ pm}^{-3}$ . Neutral atom scattering factors were taken into account. All calculations and drawings were performed with the SHELXTL PC package.<sup>18</sup> Additional material available from the Cambridge Crystallographic Data Centre, 12 Union Road, Cambridge CB2 1EZ comprises atom coordinates, thermal parameters and remaining bond lengths and angles.†

### Acknowledgements

This work was supported by the DFG, VW-Stiftung and Fonds der Chemischen Industrie.

† *Supplementary material*: see 'Instructions for Authors', in the January issue.

### References

- 1 L. E. Orgel, *J. Chem. Soc.*, 1961, 3683; A. Ceulemans and L. G. Vanquickenborne, *Pure Appl. Chem.*, 1990, **62**, 1081.
- 2 T. Ito, N. Tanaka, I. Hanazaki and S. Nagakura, *Bull. Chem. Soc. Jpn.*, 1969, **42**, 702; A. Rusina, A. A. Vlcek and S. Zalis, *Z. Chem.*, 1979, **19**, 27; C. Gooijer, N. H. Velthorst and C. MacLean, *Mol. Phys.*, 1972, **24**, 1361.
- 3 W. Kaim, *J. Am. Chem. Soc.*, 1982, **104**, 3833, 7385.
- 4 S. Ernst and W. Kaim, *J. Am. Chem. Soc.*, 1986, **108**, 3578.
- 5 W. Kaim, B. Olbrich-Deussner, R. Gross, S. Ernst, S. Kohlmann and C. Bessenbacher in *Importance of Paramagnetic Organometallic Species in Activation, Selectivity and Catalysis*, ed. M. Chanon, Kluwer Academic, Dordrecht, 1989, p. 283.
- 6 E. C. Alyea, J. Malito, S. D. Ernst, W. Kaim and S. J. Kohlmann, *Polyhedron*, 1989, **8**, 921.
- 7 W. Kaim, S. Kohlmann, S. Ernst, B. Olbrich-Deussner, C. Bessenbacher and A. Schulz, *J. Organomet. Chem.*, 1987, **321**, 215.
- 8 S. Ernst, V. Kasack and W. Kaim, *Inorg. Chem.*, 1988, **27**, 1146.
- 9 A. Klein, H.-D. Hausen and W. Kaim, *J. Organomet. Chem.*, 1992, **440**, 207.
- 10 W. Kaim and A. Klein, *Organometallics*, 1995, **14**, 1176.
- 11 J. A. Weil, J. R. Bolton and J. E. Wertz, *Electron Paramagnetic Resonance*, Wiley, New York, 1994.
- 12 W. Kaim, *Inorg. Chem.*, 1984, **23**, 3365.
- 13 W. Kaim, *Coord. Chem. Rev.*, 1987, **76**, 187.
- 14 H. tom Dieck, K. E. Franz and F. Hohmann, *Chem. Ber.*, 1975, **108**, 163.
- 15 E. Amouyal, A. Homsy, J. C. Chambron and J. P. Sauvage, *J. Chem. Soc., Dalton Trans.*, 1981, 933.
- 16 J. Fees, W. Kaim, M. Moscherosch, W. Matheis, J. Klima, M. Krejčík and S. Zalis, *Inorg. Chem.*, 1993, **32**, 166.
- 17 H. Bock and P. Hänel, *Z. Naturforsch., Teil B*, 1992, **47**, 288.
- 18 Siemens Analytical X-Ray Instruments, *SHELXTL PC*, Release 4.1, May 1990.
- 19 V. H. Houlding and V. M. Miskowski, *Coord. Chem. Rev.*, 1991, **111**, 145.
- 20 C. Vogler, B. Schwederski, A. Klein and W. Kaim, *J. Organomet. Chem.*, 1992, **436**, 367.
- 21 S. A. MacGregor, E. McInnes, R. J. Sorbie and L. J. Yellowlees in *Molecular Electrochemistry of Inorganic, Bioinorganic and Organometallic Compounds*, eds. A. J. L. Pombeiro and J. A. McCleverty, Kluwer Academic, Dordrecht, 1993, p. 503.
- 22 P. S. Braterman, J.-I. Song, F. M. Wimmer, S. Wimmer, W. Kaim, A. Klein and R. D. Peacock, *Inorg. Chem.*, 1992, **31**, 5084.
- 23 J. Fees, A. Klein and W. Kaim, unpublished results.
- 24 *cf.* E. Waldhör, M. M. Zulu, S. Zalis and W. Kaim, *J. Chem. Soc., Perkin Trans. 2*, submitted for publication.
- 25 *cf.* M. Thurnauer, J. W. Braun, P. Gast and L. L. Fezel, *Radiat. Phys. Chem.*, 1989, **34**, 647.

Paper 5/02072G

Received 31st March 1995

Accepted 7th June 1995